

Effects of *tert*-Butyl Halide Molecular Siting in Crystalline NaX Faujasite on The Infrared Vibrational Spectra

Jack D. Fox^{*,†} and Aiyakrishnan Meenakshi[‡]

Research and Development, Rochester Midland Corporation, Rochester, New York 14621, and
Department of Physics, Binghamton University, Binghamton, New York 13902

Received: August 13, 2004; In Final Form: March 14, 2005

Experimental, analytical, and modeling techniques employed in this study elucidate interactions between adsorbate molecules and the interior surfaces of the porous host faujasite. The vibrational spectroscopies of guest and host offer opportunities to locate the guest site in the host. We present Fourier transform (FT) infrared (IR) studies of sodium-X (NaX) faujasite supercage-included *tert*-butyl halides, (CH₃)₃C-X (X=Cl, Br, I) in comparison with the adsorbate molecular gas-phase and host solid-state spectra at 295 K. Four observations of guest (ν_5 , ν_6 , ν_7 , and $\{\nu_3, \nu_{16}, \nu_{17}\}$) vibrational mode changes, three of them concomitant with host mode changes, together with modeling studies, point to a particular preferred siting of the guest molecules at host hexagonal prisms (D6R). The siting involved simultaneous interactions of the host with methyl group axial protons and the halide atom. All three methyl group axial protons interact preferentially with a single D6R O1 oxygen atom via C–H···O bonding. The halide atom also interacts with a site III' Na cation. The cation, in turn, is coordinated by three O atoms (two O1 and an O4). Two of these O atoms (O1) bridge the double six-rings that form the hexagonal prism part of the NaX substructure. O4 connects the two D6R units.

Introduction

The study of interactions between molecular entities, particularly at the interface between different states of matter, is a topic whose fundamental principles and applications have had a tremendous effect upon the advancement of chemistry in the past century. The various molecular interactions govern the frequencies of molecular and intermolecular motions, which in turn dictate what processes are possible and occur with what probabilities at a given temperature. Although too numerous to mention here, some of the more notable advances include the fields of separation, heterogeneous synthesis, polymerization, heterogeneous catalysis, energy transfer, and drug design.

Synthetic faujasites are nanoporous crystalline aluminosilicate materials that are well known for their many useful catalytic and separatory applications. They are widely available in a variety of natural and synthetic forms. Of the synthetic types, dehydrated forms of the X- and Y-type faujasites have been particularly well studied, in part based on their extensive use as catalytic crude oil cracking agents by the petroleum industry.¹ These studies frequently concern the effect that modification of some controllable parameter of the faujasite, such as type of exchangeable cation or doping with another catalytic agent, has on the products of a reaction.² Somewhat less frequently, faujasites are studied in an attempt to gain insight into the nature of the various interactions that must be taking place between the guest molecules and the surfaces, cages, and channels of these ordered yet complex, highly porous solid hosts. However, studies of guest/NaX systems reported in the recent literature are beginning to reveal an understanding of these interactions with considerable detail. The crystal structure and elemental

composition of NaX is well known,³ yet the material is complex in the ways that it interacts with included guests. The literature indicates that these complexities are due primarily to the necessarily inhomogeneous distribution of silicon, aluminum, and cations (typically sodium), the extensive tetrahedral network of interconnecting pore structures, and consequently the materials' high surface areas. The three basic types of effects that govern interactions of guests in faujasites are guest interactions with cations, molecular adsorption, and the presence of adsorbed water. With regard to the study of adsorbate interactions, there is a relatively small range of molecules whose detailed interactions with NaX have been reported. Representative examples of molecular interactions with NaX and the various techniques to study them include hydrochlorofluorocarbons via nuclear magnetic resonance, X-ray and neutron diffraction⁴ and modeling studies,⁵ aromatic hydrocarbon⁶ and nitroxide⁷ free radical spin probes via electron paramagnetic resonance, methylamine by infrared spectrometry,⁸ furan by combined infrared and inelastic neutron scattering spectrometries,⁹ and water by X-ray diffraction.¹⁰ These studies have revealed often-subtle effects of guest adsorption in NaX, typically on such phenomena as coordination with Na and cation binding dynamics. However, it is more difficult to find work relating to the effects of adsorption on the aluminosilicate framework. The works with the hydrochlorofluorocarbons^{4,5} have revealed stronger interactions of fluorine with the Na cations than with aluminosilicate framework oxygen atoms, although these weaker F···O framework interactions, ascribed to van der Waals forces, were certainly present. On the other hand, the chlorine atoms were observed to interact more weakly with Na cations and more strongly with framework oxygen atoms. Weak interactions between the organic hydrogen atoms and framework oxygen were also observed. These combined X-ray, neutron and NMR results demonstrated that fluorine–sodium interactions determined siting and orientation, but in the absence of fluorine, the

* Corresponding author. Telephone (585) 336-2367, Fax (585) 336-2306, e-mail: jfox@rochestermidland.com.

[†] Rochester Midland Corporation.

[‡] Binghamton University.

chlorine-framework oxygen interactions dominated siting and orientation over the apparently weaker organic hydrogen-framework and chlorine–sodium interactions. The present work appears to show that for certain molecular geometries the chlorine–sodium interaction may predominate over the chlorine–oxygen interaction.

In an effort to learn more about the vibrational characteristics of these types of interactions, infrared spectroscopy was employed on the *tert*-butyl halides in NaX faujasite, with the halogen series spanning the chloride, bromide, and iodide. The use of the aliphatic bromide and iodide molecules was anticipated in an attempt to further study the halogen-framework oxygen interactions reported in earlier works.^{4,5} By using the aliphatic halocarbons and dehydrated faujasite, we attempt to focus attention on the molecular adsorptive effects in the current work. Computational techniques were employed to support experimental assignments and to explore the various ways in which the guests and host could interact, thereby reproducing trends in the experimental band shifts. The experimental and computational approaches have been combined into a methodology that can be utilized to obtain information from the infrared about the sites of the molecular guests within the host framework. This methodology should find general application to a variety of problems involving molecular interactions in the physical, chemical, and biological materials sciences.

Experimental Section

Detailed description of all experimental aspects can be found in the Supporting Information accompanying this work. Samples of dried NaX faujasite (Zeolyst Corp.) that had been loaded with four molecules per supercage of the halocarbon guests *tert*-butyl chloride (TBC, 99%, Aldrich), *tert*-butyl bromide (TBB, 98%, Aldrich), and *tert*-butyl iodide (TBI, 95%, Aldrich) were studied. The halocarbon guest samples were utilized as received. NaX faujasite characterization was performed via powder X-ray diffraction, X-ray elemental, and differential thermal analyses as reported in a previous work.¹¹ The X-ray elemental analysis results of the characterization produce the dehydrated unit cell formula $\text{Na}_{82}(\text{SiO}_2)_{110}(\text{AlO}_2)_{82}$ with Si/Al = 1.34, consistent with an X-type faujasite unit cell.

The loading of faujasite samples was accomplished using standard vacuum techniques. The general procedure involved gradual thermal dehydration under reduced pressure of the powder as received, followed by volatilization of the guest under its own vapor pressure into the dehydrated host. A comparison of powder X-ray diffractograms of material that was treated in this way with untreated NaX materials, both (re)hydrated to an identical level, showed no dealumination of the framework as a result of sample dehydration. X-ray diffractograms were measured on a Scintag XDS 2000 diffractometer using Cu K α radiation. The doped faujasite samples were then brought into a glovebox under a water- and oxygen-scrubbed argon atmosphere where they were handled. Fourier transform infrared (FTIR) transmission measurements on the doped faujasites were then obtained utilizing wafers prepared by the KBr dilution technique¹² at the 1% faujasite in KBr level. Wafers were pressed at 20,000-pound applied load (9.02 ton/cm²) for five minutes without evacuation. The FTIR spectrometer utilized was an Analect RFX-30 equipped with KBr optics and a Whatman model 74-5041 dry-, CO₂-free purge air source. The nominal spectral resolution was 2 cm⁻¹, 128 acquisitions were averaged, and Gaussian apodization was utilized along with three interpolated zeros per data point. Frequency accuracy of the system was calibrated versus a 38 μm thick film of polystyrene and

was found to be $\pm 1.6 \text{ cm}^{-1}$ over the spectral range from 545 to 3082 cm⁻¹. The accepted frequency values for the relevant bands were obtained from a National Institutes of Standards and Technology (NIST) document.¹³ Gas-phase spectra were acquired for each *tert*-butyl halide using a standard 10 cm cell with KBr windows.

Results

Table 1 lists the experimental spectral data for the guests gathered in the gas phase along with the included guest band values. The band positions $\bar{\nu}_o$ and the shifts $\Delta\bar{\nu}_o$ derived from them were determined from the line shape of each band. The experimental bands are assigned with the original normal mode numbering convention as developed by Wilson.¹⁴ The results in Table 1 are generally organized so that one may view any changes that were manifest in the vibrational spectra due to guest inclusion into the faujasite. This is accomplished by always referring to the shifts in vibrational band maxima of the guest in the host as $(\bar{\nu}_{o,\text{doped}} - \bar{\nu}_{o,\text{gas}})$, so that negative values of this quantity refer to a reduction in the vibrational band maximum of the guest in the host relative to its gas-phase value. For intensities, that were acquired and presented in transmittance units and were converted to standard absorbance units for fitting purposes, the most intense band for the guest in its particular environment was chosen as the denominator in a normalization factor ratio. The actual intensity value for a particular guest vibrational band in the faujasite environment is then ratioed to this normalization factor. The same procedure is applied to the matching gas-phase transition, and the difference is again taken to show reductions as negative values. This approach produces qualitative intensity results at best, but the approach can identify gross changes in the spectral intensities that may arise from interactions of the guest with the host. The approach also has the effect of compensating for some of the many general and well-known sources of error that are often encountered in quantitative infrared measurements of solid materials. Due to these uncertainties, we will make note only of percentage change values greater than $\pm 25\%$.

Least-squares fits of an appropriate line shape function were used to obtain values and uncertainties in peak positions, line widths, and intensities of all bands of interest (vapor phase guest, empty host, and guest in host). Gaussian and Lorentzian functions were both evaluated on several bands, with the Gaussian function producing the superior results as judged by the standard deviations of the fits. The Gaussian was parameterized as

$$I = I_o \exp\left[-\left(\frac{(\bar{\nu} - \bar{\nu}_o)^2}{\Delta\bar{\nu}_o^2}\right)\right] \quad (1)$$

where I_o is the intensity at $\bar{\nu}_o$, $\bar{\nu}_o$ is the frequency at the center of the band, and $\Delta\bar{\nu}_o$ is the half line width of the band at the intensity ($e^{-1}I_o$). The standard deviations of the fits were typically 2% of I_o , with Lorentzian fit errors of about twice this amount.

The parameter $\bar{\nu}_o$ is of primary interest for interpretation of interactions between the guest and host. The standard deviations of $\bar{\nu}_o$ from the Gaussian fits were typically 0.2 to 0.4 cm⁻¹. This standard deviation was propagated with the standard error from the polystyrene frequency calibration (1.6 cm⁻¹) and with the instrument's nominal resolution setting (2 cm⁻¹) as additional sources of error to produce a band position accuracy of 3 cm⁻¹ for the spectral results in this work. Simple linear error propagation of the 3 cm⁻¹ band position accuracy value

TABLE 1: Comparative Summary of the Characteristics of Eight Infrared Vibrational Bands of the *tert*-Butyl Halides (Cl, Br, and I) Adsorbed in NaX and in the Gas Phase^a, and Frequency of the Closest NaX Host Band

band type and assignment	gaussian fit parameter	TBC	TBC in NaX	shifts ^b	TBB	TBB in NaX	shifts ^b	TBI	TBI in NaX	shifts ^b	closest NaX band
C–X stretch	I_o	0.84	0.05	9	0.42	0.07	77	0.04	0.09	75	565
ν_7	$\bar{\nu}_o(\text{cm}^{-1})$	584	583	-1	525	581	56	495	570	75	
	$\Delta\bar{\nu}_o(\text{cm}^{-1})$	17	35	17	15	38	23	14	34	20	
C–C/C–X stretch	I_o	0.40	0.01	-10	0.19	0.02	17	0.04	0.02	8	756
ν_6	$\bar{\nu}_o(\text{cm}^{-1})$	816	837	21	808	824	15	805	828	23	
	$\Delta\bar{\nu}_o(\text{cm}^{-1})$	16	30	14	15	26	11	14	32	18	
C–X stretch	I_o	1.38	0.08	0	1.83	0.06	-14	0.46	0.11	-2	0.15
CH ₃ rock	$\bar{\nu}_o(\text{cm}^{-1})$	1162	1116	-46	1153	1129	-24	1147	1106	-42	1060
ν_5	$\Delta\bar{\nu}_o(\text{cm}^{-1})$	26	55	29	13	43	29	14	56	42	85
C–C stretch	I_o	0.44	<i>c</i>		0.23	<i>c</i>		0.04	<i>c</i>		1060
ν_{19}	$\bar{\nu}_o(\text{cm}^{-1})$	1235			1234			1222			
	$\Delta\bar{\nu}_o(\text{cm}^{-1})$	15			13			24			
CH ₃ C–H symmetric bend	I_o	0.83	0.01	-42	0.68	0.02	-3	0.18	0.02	-26	1641
ν_4, ν_{18}	$\bar{\nu}_o(\text{cm}^{-1})$	1376	1370	-5	1375	1370	-5	1375	1367	-8	
	$\Delta\bar{\nu}_o(\text{cm}^{-1})$	18	8	-10	14	11	-3	14	9	-5	
CH ₃ C–H antisymmetric bend	I_o	0.47	0.02	-14	0.34	0.02	-10	0.13	0.03	0	1641
$\nu_3, \nu_{16}, \nu_{17}$	$\bar{\nu}_o(\text{cm}^{-1})$	1466	1478	13	1463	1476	13	1460	1477	17	
	$\Delta\bar{\nu}_o(\text{cm}^{-1})$	24	17	-8	22	20	-2	24	31	7	
CH ₃ C–H symmetric stretch	I_o	0.80	0.05	6	0.56	0.06	48	0.30	0.07	-4	3261
ν_2, ν_{15}	$\bar{\nu}_o(\text{cm}^{-1})$	2942	2926	-16	2925	2918	-7	2927	2953	26	
	$\Delta\bar{\nu}_o(\text{cm}^{-1})$	73	89	16	56	82	26	65	110	45	
CH ₃ C–H antisymmetric stretch	I_o	1.38	0.02	-72	1.02	0.04	-2	0.42	0.05	-44	3261
$\nu_1, \nu_{13}, \nu_{14}$	$\bar{\nu}_o(\text{cm}^{-1})$	2980	2967	-13	2982	2964	-18	2976	2960	-16	
	$\Delta\bar{\nu}_o(\text{cm}^{-1})$	28	26	-2	24	38	14	27	35	8	

^a Spectra are from the 1.3–1.5 mass % *tert*-butyl halide-adsorbed NaX in a KBr wafer versus 1.0 mass % unloaded NaX in a KBr wafer. ^b Shifts are given as doped value minus gas-phase value. Intensity shifts are expressed as percentages based on experimental intensities normalized to the maximum intensity band for each spectrum. ^c No band was present at a level greater than two times the spectral noise.

results in an uncertainty of 4 cm⁻¹ for the shifts in vibrational band positions.

The assignment of normal modes to particular TBH guest experimental bands was based on a combination of existing vibrational studies in the literature for two of the *tert*-butyl halides (TBC and TBB) along with calculations of equilibrium geometry performed by us. In addition to providing confirmation of band assignments, calculations on isolated TBH molecules were performed for comparison of calculated vibrational energies of the guests to experimental gas-phase values, as well as in order to better visualize the components of guest nuclear motion that are interacting with the host when the two are brought into contact. The Microsoft Windows-based computational application TITAN (Wavefunction Inc., Irvine, CA and Schrödinger Inc., New York, NY) was utilized to generate a molecular mechanics analysis using the Merck Molecular Force Field (MMFF94)¹⁵ within TITAN's Mechanics program release 6.0.6. MMFF94 was chosen based on its empirical parametrization and hence the superior proximity of its frequency output to experimental gas-phase *tert*-butyl halide frequencies, relative to various semiempirical, Hartree–Fock, density functional, and Möller–Plesset quantum mechanical schemes available for use in TITAN. The MMFF94 analysis of equilibrium geometry was configured to generate normal coordinates and expected vibrational frequency values for all 36 vibrational normal modes for each *tert*-butyl halide. Of the 36 vibrational modes ($\Gamma_{\text{V,tot}} = 8A_1 + 4A_2 + 12E$), 32 are formally infrared-active ($\Gamma_{\text{IR}} = 8A_1 + 12E$). Figure 1 shows diagrammatical representations of all guest normal modes of vibration that are discussed in this work.

Table 2 shows a comparison between the experimental results for the eight most intense gas-phase vibrational bands of TBC, values calculated using TITAN, and those taken from the literature.¹⁶ Table 3 contains the corresponding data for TBB.¹⁷ Tables 2 and 3 illustrate the good agreement between the experimental and calculated frequencies from this study and the literature values for TBC and TBB, respectively. Gas-phase

experimental frequencies and assignments for all *tert*-butyl iodide bands were not found in a search of the literature indexed in Chemical Abstracts, making this work the only apparent direct source of infrared-active 1←0 vibrational frequencies and assignments for the entire molecule. The frequencies and their assignments are listed in Table 4. McKean et al. did report experimental data for the C–H stretching bands of TBI, but did not discuss other bands aside from C–D stretches upon deuteration.¹⁸ McKean's C–H stretching values are included in Table 4. Figure 2 shows the infrared spectra for each of the *tert*-butyl halides in NaX, along with the corresponding isolated host and guest spectra.

Table 1 reveals several interesting features of the vibrational data, both within results for the individual molecules and across the homologous series of guests in NaX.

C–X Bend and CH₃ Rock, ν_{19} . One of the more obvious observations involves the disappearance of the ν_{19} normal mode gas-phase band of symmetry species E located near 1230 cm⁻¹ for all three guests upon inclusion into NaX. The normal coordinate analysis shows that this mode is skeletal in the sense that it primarily involves displacements of only the molecular framework Cl and C atoms, and is best pictured as a superposition of C–X bending and CH₃ rocking displacements, with a smaller amount of C–C stretching as well. The CH₃ rocking displacement is best described as an alternating motion of the methyl group in the direction of the principal axis of the molecule (the C–X bond) that has no rotational characteristics of the methyl hydrogen atoms with respect to the C–CH₃ bond axis.

C–X Stretching, ν_7 . The primarily C–X stretching band ν_7 in the gas phase varies in frequency across the *tert*-butyl halide series from 584 cm⁻¹ for TBC to 525 cm⁻¹ in TBB and 495 cm⁻¹ for TBI. This well-known effect is due to the decreasing force constant of the C–X bond in going from C–Cl toward C–I. It is noteworthy that the mode also involves significant axial H atom displacements. The gas-phase trend is eliminated

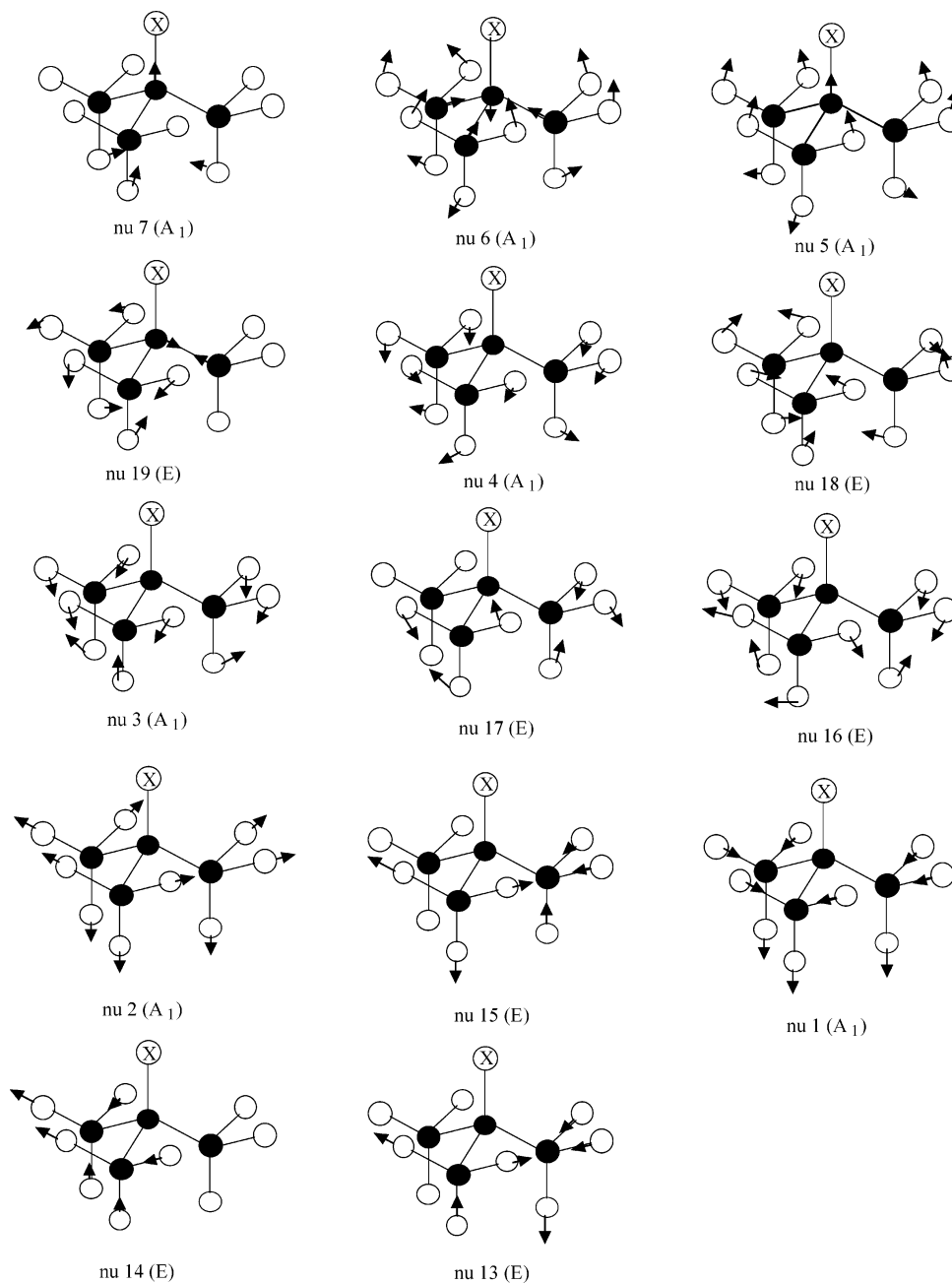


Figure 1. Diagrams of the *tert*-butyl halide vibrational normal modes discussed in this work. White = hydrogen, black = carbon, and X = halogen (neither the molecule nor the displacement arrows are drawn to scale). Only one member of a degenerate E pair is shown.

upon inclusion of the *tert*-butyl halides into NaX, with the average value for the resulting bands and their frequency spread being $578 \pm 9 \text{ cm}^{-1}$. For the ν_7 band in the guest/host system, the intensities relative to the gas-phase values increased to +37% and +74% for TBB and TBI respectively, with no significant change being observed for TBC (−5%). In addition to the intensity and blue shifts in peak position, there is also a systematic increase in the line width relative to the gas phase for the ν_7 band, from -4 cm^{-1} for TBC to $+14 \text{ cm}^{-1}$ for TBI to 20 cm^{-1} for TBI.

C–C and C–X Stretching, ν_6 . The atomic displacements during the course of the normal mode vibration ν_6 in *tert*-butyl halides are best described as a mixing primarily of C–C and C–X stretching motions, with the hydrogen atoms maintaining relatively fixed positions in space with respect to their constituent methyl carbon atoms. The frequency values for ν_6 are significantly raised by 21, 15, and 23 cm^{-1} for TBC, TBB, and

TBI, respectively, upon inclusion into NaX. Changes in the relative intensity of this band of -10 , $+17$, and $+8\%$ for TBC, TBB, and TBI, respectively, were not significant. The line widths of this band are broadened across the series also, with increases of 14, 11 and 18 cm^{-1} being observed for TBC through TBI, respectively.

C–X Stretch, CH_3 Rock, and C–H Bend, ν_5 . The band assigned to the very intense skeletal mode ν_5 near 1150 cm^{-1} in the guests is a superposition of mostly C–X stretching and bending with CH_3 rocking and C–H bending displacements. The interaction of this guest mode with a shoulder band at 1060 cm^{-1} in dry, undoped NaX to form a single “hybrid” band, upon guest inclusion into the host, can be seen for all three guests in Figure 2. The faujasite shoulder band is on the high-frequency side of the very strong faujasite framework internal Si–O–Si(Al) stretching vibration centered at 982 cm^{-1} in dry, undoped NaX. For each guest, the resultant hybrid band

TABLE 2: Comparison of the Experimental, Literature, and Calculated Vibrational Frequencies for the Eight Major Infrared Active Bands of *tert*-Butyl Chloride

band	exptl (cm ⁻¹)	Evans & Lo ¹⁶ (cm ⁻¹)	calcd ^a (cm ⁻¹)
ν_7	584	585	585
ν_6	816	818	818
ν_5	1162	1155	1174
ν_{19}	1235	1241	1216
ν_4, ν_{18}	1376	1375	1469, 1453
$\nu_3^b, \nu_{16}, \nu_{17}$	1466	1448 ^b , 1480, 1462	1470 ^b , 1470, 1467
ν_2, ν_{15}	2942	2937	2852, 2853
$\nu_{11}, \nu_{13}, \nu_{14}$	2980	2981	2955, 2955, 2953

^a Calculations were performed with TITAN/MMFF94. ^b This band was absent in the IR but strong in the Raman in Evans & Lo's study.¹⁶ Vibrational mode calculations^a in the current work show that this A₁ mode induces a significant electric dipole moment change of the molecule.

TABLE 3: Comparison of the Experimental, Literature, and Calculated Vibrational Frequencies of the Eight Major Infrared Active Bands of *tert*-Butyl Bromide

band	exptl (cm ⁻¹)	Bertie & Sunder ¹⁷ (cm ⁻¹)	calcd ^a (cm ⁻¹)
ν_7	525	524	516
ν_6	808	808	805
ν_5	1153	1153	1157
ν_{19}	1234	1238	1203
ν_4, ν_{18}	1375	1397, 1375	1467, 1452
$\nu_3, \nu_{16}, \nu_{17}$	1463	1480, 1457, 1447 ^b	1473, 1473, 1466
ν_2, ν_{15}	2925	2934, 2953	2851, 2852
$\nu_{11}, \nu_{13}, \nu_{14}$	2982	2977, 2992 (ν_{13})	2956, 2954, 2952

^a Calculations were performed with TITAN/MMFF94. ^b This band was absent in the IR but had a weak shoulder in the (liquid) Raman in the study of Bertie & Sunder.¹⁷ Vibrational mode calculations^a in the current work show that this E mode induces a significant electric dipole moment change of the molecule.

TABLE 4: Comparison of the Experimental, Literature, and Calculated Vibrational Frequencies of the Eight Major Infrared Active Bands of *tert*-Butyl Iodide

band	exptl (cm ⁻¹)	McKean et al. ¹⁸ (cm ⁻¹)	calcd ^a (cm ⁻¹)
ν_7	495		447
ν_6	805		774
ν_5	1147		1135
ν_{19}	1222		1189
ν_4, ν_{18}	1375		1465, 1451
$\nu_3, \nu_{16}, \nu_{17}$	1460		1472, 1472, 1467
ν_2, ν_{15}	2927	2909 ^b	2851, 2852
$\nu_{11}, \nu_{13}, \nu_{14}$	2976	2967 ^b	2955, 2953, 2952

^a Calculations were performed with TITAN/MMFF94. ^b These bands are discussed in terms of C–H stretching vibrations parallel (H trans to the I atom) and perpendicular (the other two methyl group hydrogen atoms) in the work of McKean et al.¹⁸ No other bands were reported or discussed in their work.

is intermediate in line width between the isolated guest and host. This observation also applies to the position of the hybrid, which is intermediate between those of the isolated guest and host. This averaging effect does not apply to the hybrid band intensity values. The relative intensity changes of the hybrid bands were only significant for the case of TBB (–50%); the changes were negligible for TBC and TBI (0 and –2% respectively).

Symmetric C–H Bending, { ν_4, ν_{18} }. The CH₃ group symmetric C–H bending band at 1375 cm⁻¹ in the gas-phase guest spectra contains contributions from the two normal modes ν_4 (symmetry species A₁) and ν_{18} (species E). The term “symmetric” refers to the cooperative, in-phase movement of all three H nuclei during the course of the vibration. For all three guests, this band moved to lower frequency upon inclusion into NaX by 5, 5, and 8 cm⁻¹ for TBC, TBB, and TBI,

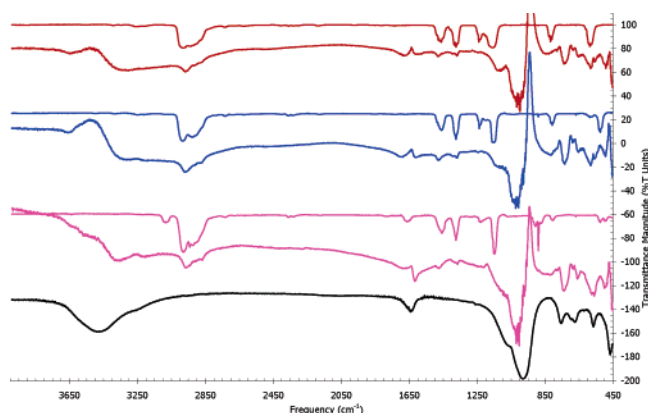


Figure 2. Infrared vibrational spectral pairs of gas-phase guest (upper) and NaX-included (lower) TBC (red traces), TBB (blue traces), and TBI (purple traces). The empty NaX host is shown as the black trace. The gas-phase guest traces are all divided by five (TBC, TBB) or three (TBI) for scaling purposes. Negative %T units are due to spectral stacking only.

respectively. The relative intensities also decreased for two of the three guests by an average of 34% (–42, –18, –26 for TBC, TBB, and TBI, respectively), with no apparent trend in the intensity reductions. In two of the three guests, the line widths for this band also significantly decreased, with values of –10, –3, and –5 being observed for the guests from TBC through TBI. Interestingly, this experimental band is the only one where a significant narrowing of its line width was observed for a majority of the guests.

Asymmetric C–H Bending, { $\nu_3, \nu_{16}, \nu_{17}$ }. The asymmetric CH₃ C–H bending band displayed shift behavior that was opposite to that of its symmetric { ν_4, ν_{18} } C–H bending counterpart mentioned above. The experimental band, which is located at an average of 1463 cm⁻¹ for the three *tert*-butyl halide guests studied, is a superposition of the C–H bending normal modes ν_3, ν_{16} , and ν_{17} . These modes are asymmetric in the sense that one of the methyl hydrogen atoms moves spatially out of phase with respect to the other two. Here the guest bands all blue shift upon inclusion into NaX, with the changes being 13, 13, and 17 cm⁻¹ for TBC, TBB, and TBI. The relative intensity changes for this band upon inclusion were not significant. The line width changes of –8, –2, and +7 cm⁻¹ for TBC through TBI do show an overall increasing trend of some 15 cm⁻¹ in line width change across the series of guests. Individually, for TBC and TBI the changes represent minor but still significant departures from the gas-phase line width values.

Symmetric C–H Stretch, { ν_2, ν_{15} }. As seen in Figure 2, the CH₃ group symmetric C–H stretching vibration band centered near 2930 cm⁻¹ appears as a very broad, noticeable shoulder on the much stronger, higher-frequency asymmetric C–H stretching band. This is observed regardless of whether the guest is in the gas phase or is included within the host environment. The symmetric stretches for the *tert*-butyl halides are assigned to the normal modes ν_2 (species A₁) and ν_{15} (species E). The gas-phase band values are slightly variable in the molecules studied, with band centers at 2942, 2925, and 2927 cm⁻¹ for TBC, TBB, and TBI, respectively. The intensity changes for { ν_2, ν_{15} } were not significant for any of the three guests upon NaX inclusion. An interesting trend in the frequency value for the shifted band maximum was observed here, with the value ranging from –16 cm⁻¹ for TBC to –7 cm⁻¹ for TBB, to +26 cm⁻¹ for TBI. The line widths for { ν_2, ν_{15} } all increased considerably upon adsorption, the increases ranging from 16 to 26 cm⁻¹ to 45 cm⁻¹ for TBC through TBI. It should

be noted that this band in the gas phase is already a factor of 2 to 4 wider than any other *tert*-butyl halide infrared band.

Asymmetric C–H Stretching, $\{\nu_1, \nu_{13}, \nu_{14}\}$. The C–H asymmetric stretching band is the highest-frequency fundamental band in the spectrum of these guests. This intense band consists of the superposition of normal modes ν_1 (A_1), ν_{13} , and ν_{14} (E).

The bands for each guest, the maxima of which are located at 2980, 2982, and 2976 cm^{-1} for TBC through TBI, all move to lower frequency upon NaX inclusion by 13, 18, and 16 cm^{-1} , respectively. It is interesting to note that for two of the three guests, the intensity changes are significantly negative by an average of 59%; the change for the other guest band is -23% (TBB). The line width changes are significant for two of the three guests (TBB and TBI) as well, where the increase was an average of 11 cm^{-1} .

Discussion

Since $\bar{\nu}_0$ is the parameter of primary interest in the interpretation of interactions between the guest and host, we will focus our discussion on changes in frequency position of the various bands. Changes in the relative intensities and bandwidths will be addressed within the context of discussions concerning the individual bands.

C–X Stretching, ν_7 . Referring to the results listed in Table 1, the relatively intense guest band ν_7 is assigned to the so-called C–X stretching motion. The spectral data reveal that this band is no longer observed at or near its gas-phase position upon inclusion into NaX, except for TBC. Rather, what is observed is a single band, in which the guest and “host” band merge and take the form of a host band pulled 5 to 19 cm^{-1} to lower frequency, in the direction of the gas-phase TBH ν_7 frequency. If we compare the observed peak position of this band to the vapor phase TBH values, we obtain a net increase in the frequency values of -1 , $+56$, and $+75$ cm^{-1} for TBC, TBB, and TBI, respectively. These changes are insignificant for the case of TBC, but large indeed for TBB and TBI. Given the large intrinsic relative intensity of the C–X stretching band in the gas-phase guest spectra and the observed movement of the faujasite 565 cm^{-1} band upon guest inclusion, it seems likely that an interaction is taking place between these vibrations to form a hybrid band.

In cases where an interaction between guests and NaX is observed^{4,8,9} or calculated,⁵ the phenomenon is frequently assigned to interactions of the guests with lattice oxygen atoms. The faujasite structure and cage sizes relative to the TBH guest sizes dictate that such an interaction would likely be with the framework O atoms that point in toward the center of the supercage or with Na cations. The supercage structure is replete with this type of oxygen atom and site III' cations. Based on atomic polarizability considerations¹⁹ and on previous studies,^{4,5} one would expect interactions between lattice O atoms and halogens to decrease in the order $\text{I} > \text{Br} > \text{Cl}$ if the interactions were dispersion-type in nature, which is in agreement with the observed trend. The strength of the observed interaction increases in magnitude as one traverses the halogen series from Cl to I. This behavior is generally consistent with the nature of the London dispersion interaction, which is directly proportional to the product of the static polarizabilities of the interacting moieties.²⁰ However, if the interaction were derived from a dipole–dipole or other type of Coulombic interaction, for example between the local Si–O–Si dipole moment of a protruding faujasite O atom or the Na cation charge and the dipole moment of TBH, one might expect the interaction to be the strongest for TBC based on its larger dipole moment and weakest for TBI. This is contrary to our experimental results.

Thus, the guest ν_7 trend at first sight appears to indicate a dispersion interaction between the C–X bond and an atom of the faujasite supercage without a formal charge, such as the oxygen atoms in the guest–host complex. The trend does not appear to support an interaction of the halide ion with the Na cation, which is predicted by molecular modeling calculations discussed in the last section, except in the unlikely event that the dispersion interaction exceeds the Coulombic interaction. The 565 cm^{-1} faujasite band has previously been assigned to pseudolattice vibrations of the hexagonal prisms (sometimes referred to as D6R secondary building units) that predominate in the faujasite structure type.²¹ This type of absorption is distinct from a normal lattice phonon mode in that only part of the lattice, in this case the hexagonal rings, possesses significant nuclear motion. A truly interesting aspect of this very specific ν_7 -D6R interaction relates to the strong suggestion of an actual interaction site between the guest and host among many different possible interaction sites. Specifically, this observation points to a guest interaction with a host O atom located on a supercage hexagonal ring site not occupied by a site II' Na ion, with a host O atom located on a supercage four-ring adjacent to a hexagonal ring, or, less likely, with a site III' cation coordinated by oxygen atoms of these rings. However, the modeling calculation to be described below suggests that the mass variation between the halides could also give rise to this effect through an attractive interaction between the axial methyl protons and an atom of these ring systems protruding into the supercage.

C–C and C–X Stretching, ν_6 . At first glance, the guest C–C/C–X skeletal stretching mode ν_6 centered near 810 cm^{-1} in the gas-phase guest spectra seems to disappear in the spectra of the doped faujasite materials. However, a closer inspection of the region around this band reveals a weak, but discernible, broadened absorption at higher frequencies than gas-phase ν_6 . Moreover, this weak, broad band exhibits a blue shift for all three guests by an average of 20 cm^{-1} , as is shown in Table 1. This fact led us to inspect this region more closely for any additional bands or movement of other spectral bands in the immediate region. The band closest to ν_6 in the spectra of the uncombined materials is a fairly intense faujasite band located at 756 cm^{-1} in dehydrated, unloaded NaX. This band has been previously assigned as a hybrid type between vibrations of the four-ring structures (S4R) and Si–O–Si bridging oxygen bending modes.²¹ For brevity, we will refer to it as S4R. In all three spectra of TBH included into NaX, we observe S4R to red shift in a remarkably consistent manner, to the value 734 ± 1 cm^{-1} . This is a decrease of 22 cm^{-1} , which within experimental error is equal to the increase observed for the ν_6 bands of the guests.

These observations can be explained by invoking a simple vibrational coupling model of two harmonic oscillators. This can be viewed as an interaction with force constant k_{12} between two harmonic oscillators with reduced masses μ_1, μ_2 , and force constants k_1, k_2 . The well-known solution of this problem²² is given by eq 2. Note that the two observed frequencies of the coupled interaction

$$\omega^2 = \frac{F_{11} + F_{22}}{2} \pm \frac{1}{2} ((F_{11} - F_{22})^2 + 4F_{12}^2)^{1/2}$$

with

$$F_{11} = \frac{k_1 + k_{12}}{\mu_1}, F_{22} = \frac{k_2 + k_{12}}{\mu_2}, F_{12} = F_{21} = \frac{-k_{12}}{(\mu_1\mu_2)^{1/2}} \quad (2)$$

Here, ω_+ and ω_- will also depend on the reduced masses μ_1 and μ_2 as well as the force constants of the two uncoupled oscillators. This theory gives two frequencies that have each increased or decreased by amounts that depend on the coupling force constant k_{12} . The difficulty in determining the reduced masses of the S4R and guest ν_6 modes prevents us from solving for k_{12} . However, using eq 2 it is possible to equate the sum of ω_+^2 and ω_-^2 with the sum of F_{11} and F_{12} . This relation can have a factor of $k_{12}[(\mu_1+\mu_2)/\mu_1\mu_2]$ separated out. Combining this result with the experimental values for the free (where $k_{12} = 0$) and coupled frequencies produces a value for $k_{12}[(\mu_1+\mu_2)/\mu_1\mu_2]$ of 7.09×10^{23} dyne \cdot cm $^{-1}\cdot$ g $^{-1}$. This value probably indicates a relatively small adsorbate–host coupling constant, as would be expected. Experimentally, we obtain 783 cm $^{-1}$ for the quantity $[(F_{11}+F_{22})/2]$ when the oscillators are free, and also $1/2((F_{11} - F_{22})^2 + 4F_{12}^2)^{1/2} = \pm 48$ cm $^{-1}$ for the coupled oscillators in the ν_6 -S4R system. The fit of the ν_6 and S4R experimental results to this type of simple harmonic model of adsorbate–host interaction is very satisfying.

C–X Stretch, CH₃ Rock, and C–H Bend, ν_5 . The band assigned to the guest skeletal mode ν_5 at an average position of 1154 cm $^{-1}$ for the three TBH molecules, which is a superposition of mostly C–X stretching with C–CH₃ group bending displacements, can be seen to interact with a shoulder band at 1060 cm $^{-1}$ on the very strong faujasite framework internal Si–O–Si(Al) stretching vibration centered at 982 cm $^{-1}$ in dry, undoped NaX. The general appearance and position of the resulting band is very reminiscent of spectral effects produced by an exchange process, for example, as one frequently sees via ^1H nuclear magnetic resonance in mixtures of molecules with labile protons chemically exchanging at intermediate time scales with respect to the measurement process. The type of exchange envisioned for the current system would similarly be a stochastic, incoherent type where, in this case, the relevant vibrational quanta of the guest and host are randomly exchanged by the phonon motions of the host lattice, thus conserving energy. A comparison of the individual results for the series of *tert*-butyl halides with each other reveals the possibility of the ν_5 -faujasite hybrid band in the TBH/NaX system being exchange-type in nature. In each case, the resultant spectral feature is significantly broadened and shifted to intermediate, nearly central, frequency values with respect to the separate halide gas-phase and undoped host values. In an attempt to evaluate semiquantitatively whether there was any type of exchange-like character to the hybrid band, we modeled the band between TBC and NaX with a simple type of exchange theory similar to the one presented by McConnell.²³ The two limiting exchange rate scenarios possible are reflected in equations 3a and 3b below.

$$\omega_{\text{obs}} = \bar{\omega} \pm ((\omega_a - \omega_b)^2 - 8P^2)^{1/2} \quad (3)$$

slow exchange, $P \ll (\omega_a - \omega_b)$: $\omega_{\text{obs}} =$
 $\bar{\omega} \pm (\omega_a - \omega_b)$; $\Delta\omega_{1/2} \approx P \approx 1/T_2$ (3a)

fast exchange, $P \gg (\omega_a - \omega_b)$: $\omega_{\text{obs}} =$
 $\bar{\omega}$; $\Delta\omega_{1/2} \approx \frac{(\omega_a - \omega_b)^2}{8P} \approx 1/T_2$ (3b)

The theory is based on a modified form of the Bloch equations²⁴ where the modified version accounts for the effect of exchange on relaxation rates, and thus the spectral line shape. In this theory ω_{obs} is the angular frequency of the exchanging states, $\bar{\omega} = (\omega_a + \omega_b)/2$ is the average frequency of the unexchanged

bands of frequencies ω_a and ω_b , P is the jumping rate (exchange frequency) of quanta between the two states, $\Delta\omega_{1/2}$ is the half-line width in wavenumbers at half-maximum of the exchanged band, and T_2 is the characteristic time for vibrational excited-state exchange of quanta *between the guest and host vibrational modes*. Prior to coalescence, the bands broaden and move closer together with increasing exchange frequency, as dictated by the general eq 3. This equation also shows that the exact condition for coalescence of the two bands occurs when the exchange rate P exceeds $(\omega_a - \omega_b)/(2(2)^{1/2})$. After coalescence, the exchange effects manifest themselves primarily as line width changes in the merged band. Using the observed values for TBC in NaX of $(\omega_a - \omega_b) = 102$ cm $^{-1}$ and $\Delta\omega_{1/2} = 55$ cm $^{-1}$, one cannot reproduce $\Delta\omega_{1/2}$ and keep the necessary condition $P > (\omega_a - \omega_b)$ for coalescence to be observed. However, if the homogeneous line width is 36 cm $^{-1}$ or less in the overall TBC/NaX ν_5 line width, the coalescence condition is satisfied.

The above equations for exchange effects on the vibrational line width assume that the only source of line broadening present is the homogeneous component due to the vibrational quantum exchange. This is not a realistic assumption for TBH in NaX. This can be verified by comparison of the guest line widths for TBH in NaX with their gas-phase values. All guest bands (with the exception of the two C–H bending bands, *vide infra*) broaden upon inclusion into NaX. The average broadening of the six bands over all three guests upon inclusion was 21 cm $^{-1}$. This broadening is most likely inhomogeneous in nature and is probably due to phonon bands and to multiple siting, such as would be caused by the random disposition of Si and Al atoms in the host metal sites. The contribution of inhomogeneous broadening to IR bands of samples in the liquid state from room temperatures down through the amorphous glass transition to 10 K has been recently measured by pulsed IR spectroscopy.²⁵ This pulsed IR work on the system W(CO)₆ in three different glass forming solvents shows that typical liquid-state homogeneous line widths are of the order of 1 to 2 cm $^{-1}$. Thus we propose that the observed averaging of the guest and host bands, in view of the expected relatively small homogeneous line widths, supports the interpretation in terms of an exchange process. Variable temperature and/or photon spin-echo measurements should be utilized to confirm the exchange nature of this assignment. We suggest that the physical basis for the proposed exchange mechanism is from phonon modes of the order of 100 cm $^{-1}$ whose stochastic activation and deactivation accompany the exchange of vibrational excitation between guest and host modes, so as to conserve energy. It is most interesting to note that there are two infrared-active phonon modes in NaX at 95 and 104 cm $^{-1}$, and also two Raman-active phonon modes at 100 and 108 cm $^{-1}$. All four of these modes have been previously assigned to SiO₄ and AlO₄ rotational lattice modes.²⁶

The faujasite band in interaction with TBH ν_5 is a relatively weak but still distinctly observable shoulder band at 1060 cm $^{-1}$ in the infrared. This band in the past has been simply assigned by many authors as part of the faujasite asymmetric Si–O–Si(Al) stretching band. This band is also present in the infrared spectra of twenty-five distinctly different zeolite structure types, contained within six distinct structural groups, studied in a recent work.²¹ Unfortunately, no more specific assignment of the 1060 cm $^{-1}$ band is available.

It is noteworthy in discussing the dynamic effect observed here that we have observed no instances where there is doubling

of any of the molecular vibration peaks that would suggest multiple siting or diffusion between several sites on a slower time scale.

Symmetric C–H Bending, $\{\nu_4, \nu_{18}\}$. The symmetric methyl C–H bending band at 1375 cm^{-1} for TBH guests is assigned to the ν_4 and ν_{18} normal modes of motion. In the IR spectra of the gas-phase guests, and more generally in most molecules containing methyl groups bonded to a carbon atom, the frequency position of this band is remarkably stable, being observed at 1375 cm^{-1} in almost every case. The reductions in frequency value for this band (5, 5, and 8 cm^{-1}) seen in the current work are unusual and represent a weakening of the symmetric bending force constant as a result of the interaction with NaX.

Asymmetric C–H Bending, $\{\nu_3, \nu_{16}, \nu_{17}\}$. A larger blue shift is observed for the CH_3 C–H antisymmetric bending band $\{\nu_3, \nu_{16}, \nu_{17}\}$ upon inclusion into NaX. This band increases its frequency value by 13, 13, and 17 cm^{-1} , as a result of its interaction. In addition, there is no significantly discernible trend in the frequency shift across the series of *tert*-butyl halides. The positive shift in peak position here indicates a strengthening of the C–H antisymmetric bending force constant. The $\{\nu_3, \nu_{16}, \nu_{17}\}$ band arises from the hydrogen displacements where one of the methyl hydrogen atoms moves spatially out of phase with respect to the other two.

Taken together, we have observed a shifting of the $\{\nu_3, \nu_{16}, \nu_{17}\}$ antisymmetric bending band to higher frequency while the symmetric C–H bending band $\{\nu_4, \nu_{18}\}$ has shifted to lower frequency. This increased separation between the symmetric and antisymmetric bending modes of the molecule could suggest a type of host-induced intramolecular vibrational coupling between these normal modes of the free molecule. As evidenced from the analysis of other modes and from molecular modeling to be described later, there are interactions of both the axial and (to a lesser extent) equatorial methyl protons with FAU O atoms of types O1 and O4. These interactions, directed at both types of proton on each of the involved methyl groups, would be expected to effect the splitting between the symmetric and antisymmetric bending modes.

Symmetric C–H Stretch, $\{\nu_2, \nu_{15}\}$. The symmetric C–H stretching band $\{\nu_2, \nu_{15}\}$ displays a unique trend in peak position upon inclusion of guest in the host, with shift values ranging from -16 cm^{-1} for TBC to -7 cm^{-1} for TBB, and to $+26\text{ cm}^{-1}$ for TBI. The fact that the band shifts show a trend from blue shifted to red shifted, as an apparent function of halide atom (i.e., polarizability), perhaps suggests the dispersion effect as the responsible interaction mechanism. Coupling through the halide atom or the axial methyl protons to the host then rearranges the normal modes, perhaps having the observed systematic effect on the C–H stretch.

C–X Bend and CH_3 Rock, ν_{19} . A currently unexplained change in the guest spectra upon inclusion relates to the disappearance of the C–X bending/ CH_3 rocking skeletal band ν_{19} . It is not immediately obvious why this band would unilaterally disappear from the spectrum. The possibility that the disappearance of ν_{19} was caused simply by its maximum molar absorptivity ϵ not being large enough can be reasonably dismissed by noting that, for all three guests, ν_{19} has an inherent intensity very close to that of the C–H bending band $\{\nu_3, \nu_{16}, \nu_{17}\}$, which is notably present in all three spectra of the guests included into NaX. The phenomenon of vibrational band disappearance has been observed previously²⁷ and is typically assigned to changes in the chemical nature of the species or to changes brought about in the effective structure and/or bonding

of the molecule as a result of its interaction with another moiety. It seems very unlikely that a structure change of *tert*-butyl halide would be the cause of this disappearance in our case, as one would expect to observe similar and/or drastic changes in the other two skeletal modes ν_5 and ν_6 as well. Chemical reaction of the *tert*-butyl halides within the faujasite framework is equally unlikely based on previous IR and microwave dielectric spectroscopic studies that show no appreciable decomposition of TBH in X- and Y-faujasites under the relatively mild conditions utilized in these types of experiments. Thus, it would appear that the band has somehow disappeared as a result of the molecule's interaction with the faujasite. Exactly how the particular interaction with the host found in this work and confirmed by modeling, to be described next, would affect a disappearance of ν_{19} is unclear.

Modeling Calculations. A variety of red and blue shifts of the TBH C–H stretching and C–H bending modes observed upon incorporation into the FAU pore structure have been described above. Hydrogen bonding is frequently associated with red-shifted C–H stretching modes. A dispersion-based, so-called, anti-hydrogen bonding²⁸ interaction and a dipole–dipole electrostatic interaction²⁹ have been proposed for blue-shifted C–H stretching modes. Fewer attempts have been made to rationalize red- and blue-shifted C–H bending modes. In an attempt to understand and predict the observed shifts of the C–H stretching and bending modes, calculations of equilibrium geometries and vibrational frequencies and their intensities were performed on a single *tert*-butyl halide molecule, both isolated and when contained within one unit cell of NaX FAU. The Materials Studio simulation environment MS Modeling 2.2 (Accelrys Inc., San Diego, CA) was employed to perform geometry optimizations and vibrational analyses using the COMPASS molecular mechanics force field³⁰ within the Discover molecular simulation program. An initial example unit cell framework structure of FAU with Si/Al = 1 in space group *Fd3*, provided within the MS Modeling package, was utilized. The Si, Al, and O atoms of this structure were charged per values published previously for zeolite potential calculations.³¹ Partial charges for the *tert*-butyl halides were calculated using a BLYP exchange/correlation potential via the DMol³ density functional module³² within MS Modeling 2.2. Na cations were placed into the FAU structure by averaging the seven distinct sites of Na cation recently reported³ into the three more commonly used subsets of types I', II, and III',⁴ followed by deletion of 64 of the 96 crystallographic SIII' sites in order to balance the charge and maximize the cation–cation distances. All Na cations were assigned a charge of +1. An energy-minimized set of geometrical coordinates then was produced for the *tert*-butyl halide guest in the Na-X host by allowing the molecule to interact with the FAU unit cell through a variety of starting orientations and positions. The results of these calculations organized themselves into energy sets such that the preferred minimum orientation repeated itself over several calculations from different starting positions, and that the next lowest-energy minimum geometry was $8.5\text{ kJ}\cdot\text{mol}^{-1}$ higher in energy. The general approach for these calculations was to freeze the host atomic positions prior to geometry optimization and subsequent frequency calculations. The resulting set of minimized coordinates was then compared with the conclusions from the vibrational analyses.

The minimum-energy set of coordinates is shown in Figure 3. All three methyl group axial protons can be seen to preferentially interact with a single D6R O1 oxygen atom. This interaction would be expected to alter the vibrational energies

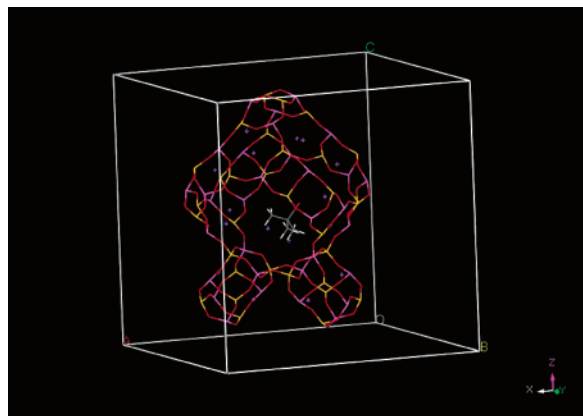


Figure 3. Truncated view of a preferred siting and orientation of TBB above a hexagonal prism (D6R) in the NaX FAU unit cell (entire cell contents not shown) as determined by the Materials Studio calculations. The D6R on the lower left bears the O1 oxygen atom interacting with (closest to) the axial hydrogen atoms of the guest. The D6R on the right shows the spatial relationship of D6R units to each other and the supercage. Host color scheme: yellow = silicon, purple = aluminum, red = oxygen, blue = sodium. Guest color scheme: gray = carbon, white = hydrogen, red = bromine.

of the guest C–H modes as well as those of the hexagonal prisms if there were a physical coupling between them, as the guest ν_6 –host S4R results demonstrate. The halide atom of the guest also interacts with a site III' Na cation that is coordinated to three O atoms (O1–O4–O1). Two of the O atoms (type O1) bridge the double six-rings that form the hexagonal prism part of the NaX substructure, while type O4 connects the two D6R units via a single S4R ring. One can see through the coordinates of this interaction the possibility that the guest C–X stretching vibrational mode ν_7 is also interacting via the Na SIII' cation with the hexagonal prism. However, the modeling results are problematic in view of the observed apparent polarizability dependence of the hybrid band between them, because it seems somewhat unlikely that the halogen–Na cation dispersion interaction exceeds the Coulombic type. Thus it is evidently not the C–X stretching aspect of ν_7 that is responsible for the dispersion-like trend, given the structure in Figure 3. We therefore explored the effect of the methyl axial $H_{\text{axial}}-O_{\text{zeo}}$ interaction with TITAN modeling calculations. We noted that the C– H_{axial} amplitudes increase systematically with halide mass in the free TBX molecule series. So prompted, we further showed with TITAN modeling calculations that when a test O_{zeo} atom (using H_2O) is brought to an equilibrium interaction with the H_{axial} atoms, ν_7 shifts from its free molecule value in the observed trend and with observed magnitudes. Our conclusion is that the $H_{\text{axial}}-D6R O_{\text{zeo}}$ interactions are sufficient to predict the modifications of guest and host vibrational energy levels reported in this work, while the TBH halide atoms interact with the Na III' ions coordinated to the zeolite O atoms associated with hexagonal prisms.

As a qualitative check on the feasibility of the coordinates produced from molecular modeling, powder X-ray diffractograms were acquired on the *tert*-butyl bromide-loaded and undoped NaX samples. Indexing of the reflections out to $2\theta = 45^\circ$ of the loaded and unloaded NaX samples produces the cubic unit cell parameter $a = 24.97 \pm 0.02$ and 24.74 ± 0.09 Å, respectively. These values are consistent with a FAU unit cell and the slight swelling in cubic unit cell parameter that occurs as a result of guest loading. The experimental diffractograms were compared to those simulated using the guest coordinates from previous geometry optimizations with the Powder Dif-

fraction tool in the Reflex module of Materials Studio 2.2. The diffractograms were simulated by entering the minimized guest atom coordinates into an $Fd\bar{3}$ FAU unit cell that had been appropriately built (again using an averaged set of Olson's coordinates³ for Na). The atom occupancies of the 96 symmetry copies of the guest coordinates were then adjusted to account for the smearing of electron density (i.e., crystallographic disorder) that would be present under the conditions of loading at 1, 2, 3, and 4 TBB molecules per supercage (occupancies were also adjusted for SIII' Na). A full-blown X-ray structure refinement is clearly beyond the scope of the current infrared vibrational analysis. The experimental intensity changes between doped and undoped reflections of the 10 most intense reflections between the (2θ) angles of 10° and 35° were compared with the simulation by normalizing each intensity change to that of the undoped reflections' intensity. As judged by a reasonably linear correlation between experimental and simulated intensity changes, the simulated results for a loading of 3–4 TBB per supercage gave the best overall agreement with respect to intensity change for those reflections whose intensities increase upon loading the TBB (all experimental reflections did increase upon TBB loading for our system). Also examined was a ~ 13 kJ/mol higher-energy local minimum interaction in which a similar interaction was present with the methyl group hydrogen atoms, and in which the halogen interacted directly with a 6-ring host oxygen. The X-ray powder diffraction simulation for the TBB located in this minimum was much less satisfactory. Encouragingly, preliminary results from the inclusion of these same *tert*-butyl halides into low-aluminum H–Y FAU, with Si/Al = 40, to be the subject of another publication, corroborate many of the conclusions presented in this paper insofar as one would expect for the differences between the hosts.

Summary

The $1 \leftarrow 0$ vibrational states of the *tert*-butyl halides $(CH_3)_3C-X$, where X = Cl, Br, and I, collectively denoted TBH, have been examined in the gas phase and upon their inclusion into the synthetic faujasite NaX (Si/Al = 1.34) at a loading level of four molecules per supercage. The vibrational states were observed at room temperature utilizing Fourier transform infrared spectrometry in the mid-infrared frequency range from 450 to 4000 cm^{-1} with a nominal spectral resolution of 2 cm^{-1} .

We have observed several interactions involving the molecular guests and the NaX host, as evidenced by resulting band energy, width, and line shape changes. The absorption bands of the guests, hosts, and the bands resulting from their interactions were fit with a Gaussian line shape function in order to determine accurately the magnitudes of peak position, intensity, and line width changes, and their associated errors. Adsorption effects on vibrational energies range up to 77 cm^{-1} . The bands assigned to guest C–X and skeletal vibrations generally shift to the largest extent, with the maximum frequency changes being observed for the guest C–X stretching band ν_7 . Similar types of change are also observed for certain bands of the host, several of which can be assigned to specific host group coordinates.

These changes thus reveal actual sites of interaction between the guests and host. Evidence is presented that supports the assignment of the shifts of the TBH ν_7 C–X stretching band to a halide mass-dependent interaction between the guest axial methyl protons and host hexagonal prism (or double six-membered ring, D6R) oxygen atoms. For all three *tert*-butyl halides, the C–C/C–X stretching band ν_6 is also involved in

an interaction with a specific host band in NaX that arises from a superposition of single four-membered ring (S4R) vibrations and Si—O—Si(Al) bending displacements. The interaction shifts the guest and host bands to an equal and opposite extent, and is thus treated using the simple physical model of two separate harmonic oscillators loosely joined by the interaction. Analysis of guest C—H displacement bands has revealed shifts in their frequencies that are indicative of interactions between the hydrogen atoms of the guests and host oxygen atoms. The C—X stretching, CH₃ rocking, and C—H bending skeletal mode, ν_5 , is seen to undergo stochastic incoherent exchange of its vibrational quantum with a feature in the faujasite asymmetric Si—O—Si(Al) stretching band. The exchange appears to be promoted by a host phonon mode, of which four are known to have the requisite energy. Temperature dependence experiments should be undertaken to corroborate the exchange character of this interaction. The frequencies of the symmetric, $\{\nu_4, \nu_{18}\}$, and asymmetric, $\{\nu_3, \nu_{16}, \nu_{19}\}$, C—H bending modes are seen to be further split away from one another upon interaction with the host. Modeling studies suggest that the three methyl group axial protons preferentially interact with a single D6R O1 oxygen atom via a weak C—H...O type of hydrogen bonding. The halide atom also interacts through a site III' Na cation with three O atoms (O1—O4—O1). Two of the O atoms (type O1) bridge the double six-rings that form the hexagonal prism part of the NaX substructure, while type O4 connects the two D6R units via a single S4R ring. This predicted interaction would give rise to the observed polarizability dependence of the hybrid band between guest ν_7 and host D6R, only in the unlikely event that the dispersion interaction with the Na ion exceeds the Coulombic contribution. Quantitative estimates indicate that this is indeed not the case. Rather, this experimental work and the modeling calculations suggest that the ν_7 effect is caused by the halide ν_7 mass dependence of the TBH axial proton interaction with the O1 host atom. Thus this experimental work and the modeling calculations leave open the cause of the apparent dispersion-like dependence of the halogen atom interaction with the host. The symmetric C—H stretching band, $\{\nu_2, \nu_{15}\}$, displays increasingly positive shifts mirroring the increasing polarizability of the halide atom. The increasing halide-D6R oxygen atom interaction may result in a reorganization of the normal modes so as to increase the split in the frequencies of these two modes. Overall, the preferred interactions for the *tert*-butyl halide/NaX system are a combination of the cation-mediated halogen—oxygen dispersion interaction and the axial methyl proton hydrogen bonding with hexagonal prisms via host oxygen atoms O1.

To our knowledge, infrared spectrometry has not been utilized to extract the types of specific siting information of guests included within hosts that are discussed in this work. A clear relationship has been established, observable in the infrared, between structural aspects of host—guest systems that can be utilized to site molecules without the use of more expensive and less widely available X-ray, neutron, and solid-state NMR techniques. The success of the infrared technique as a tool for molecular siting provided the basis for initiation of the molecular modeling studies described in the preceding section. The modeling studies illustrate how computational results can be employed to seek a more complete understanding of experimental vibrational spectra. The results suggest additional studies to ascertain the general applicability of the described methods of vibrational spectroscopy and analysis to other types of host—guest systems.

Acknowledgment. The authors thank Professor David C. Doetschman of Binghamton University (State University of New York) for countless invaluable discussions regarding the results of this work and their interpretation. Thanks are also due to Dr. Szu-Wei Yang, who provided the *tert*-butyl iodide-included faujasite samples. The generous hospitality of Dr. Donald P. Wyman, Sr. Vice President and Director of Research and Development for Rochester Midland Corporation, is greatly appreciated for time necessary to conduct and complete this work. We thank Dr. Peter Zavalij for his assistance in obtaining the X-ray powder diffraction spectra and his advice.

Supporting Information Available: A detailed experimental procedure, *tert*-butyl halide vibrational band intensity calculations, and powder X-ray diffractograms of NaX at various stages of treatment and guest loading are presented. This material is available free of charge via the Internet at <http://pubs.acs.org>.

References and Notes

- Breck, D. *Zeolite Molecular Sieves*, Wiley: New York, 1974.
- Sivaguru, J.; Natarajan, A.; Kaanumalle, L.; Shailaja, J.; Uppili, S.; Joy, A.; Ramamurthy, V. *Acc. Chem. Res.* **2003**, *36*, 509.
- Olson, D. *Zeolites* **1995**, *15*, 439.
- Ciraolo, M.; Hanson, J.; Toby, B.; Grey, C. *J. Phys. Chem. B* **2001**, *105*, 12330.
- Jaramillo, E.; Grey, C.; Auerbach, S. *J. Phys. Chem. B* **2001**, *105*, 12319.
- Doetschman, D.; Dwyer, D.; Fox, J.; Frederick, C. F.; Scull, S.; Thomas, G.; Utterback, S.; Wei, J. *Chem. Phys.* **1994**, *185*, 343.
- Doetschman, D.; Thomas, G. *Chem. Phys.* **1998**, *228*, 103.
- Docquir, F.; Toufar, H.; Su, B. *Langmuir* **2001**, *17*, 6282.
- Beta, I.; Jobic, H.; Geidel, E.; Böhlig, H.; Hunger, B. *Spectrochim. Acta A* **2001**, *57*, 1393.
- Kirschhock, C.; Hunger, B.; Matrens, J.; Jacobs, P. *J. Phys. Chem. B* **2000**, *104*, 439.
- Borkowski, R.; Doetschman, D.; Fox, J.; Gargossian, C. *Solid State Ionics* **1997**, *100*, 95.
- Stimson, M.; O'Donnell, M. *J. Am. Chem. Soc.* **1952**, *74*, 1805.
- Gupta, D.; Wang, L.; Hanssen, L.; Hsia, J.; Datla, R. **1998**, SRM 1921, NIST Special Publication 260-122.
- Wilson, E., Jr. *Phys. Rev.* **1934**, *45*, 706.
- Halgren, T. *J. Comput. Chem.* **1996**, *17*, 490.
- Evans, J. Jr., Lo, G. *J. Am. Chem. Soc.* **1966**, *88*, 2118.
- Bertie, J.; Sunder, S. *Can. J. Chem.* **1973**, *51*, 3344.
- McKean, D.; Biedermann, S.; Bürger, H. *Spectrochim. Acta* **1974**, *30*, 845.
- Weast, R. (Ed.-in-Chief), *CRC Handbook of Chemistry and Physics*, 70th ed.; CRC Press: Boca Raton, 1989; pp. E-72, E-76.
- Berry, R.; Rice, S.; Ross, J. *Physical Chemistry*, 2nd ed.; Oxford: New York, 2000; p. 303.
- Mozgawa, W. *J. Mol. Struct.* **2001**, *596*, 129.
- Wilson, E., Jr.; Decius, J.; Cross, P. *Molecular Vibrations The Theory of Infrared and Raman Vibrational Spectra*; Dover: New York, 1980; pp. 27-31, 52, 161.
- McConnell, H. *J. Chem. Phys.* **1958**, *28*, 430.
- Bloch, F. *Phys. Rev.* **1946**, *70*, 460. Bloch, F.; Hansen, W.; Packard, M. *Phys. Rev.* **1946**, *70*, 474.
- Tokmakoff, A.; Fayer, M. *J. Chem. Phys.* **1995**, *103*, 2810.
- Butler, W.; Angell, C.; Allister, W.; Risen, W. *J. Phys. Chem.* **1977**, *81*, 2061.
- Urban, M.; Salazar-Rojas, E. *J. Appl. Polym. Sci.* **1990**, *28*, 1593.
- Hobza, P.; Havlas, Z. *Chem. Phys. Lett.* **1999**, *303*, 447.
- Hobza, P.; Spirko, V.; Havlas, Z.; Buchhold, K.; Reimann, B.; Barth, H.; Brutschy, B. *Chem. Phys. Lett.* **1999**, *299*, 180.
- Sun, H. *J. Phys. Chem. B* **1998**, *102*, 7338.
- Jaramillo, E.; Auerbach, S. *J. Phys. Chem. B* **1999**, *103*, 9589.
- Delley, B. *J. Chem. Phys.* **2000**, *113*, 7756. Delley, B. *J. Chem. Phys.* **1990**, *92*, 508.